



Missouri University of Science and Technology
Scholars' Mine

International Specialty Conference on Cold-Formed Steel Structures

(2012) - 21st International Specialty Conference on Cold-Formed Steel Structures

Aug 24th, 12:00 AM - Aug 25th, 12:00 AM

Direct Strength Design of Metal Building Wall and Roof Systems - Through-fastened Simple Span Girts and Purlins with Laterally Unbraced Compression Flanges

Tian Gao

Cristopher D. Moen

Follow this and additional works at: <https://scholarsmine.mst.edu/isccss>

 Part of the [Structural Engineering Commons](#)

Recommended Citation

Gao, Tian and Moen, Cristopher D., "Direct Strength Design of Metal Building Wall and Roof Systems - Through-fastened Simple Span Girts and Purlins with Laterally Unbraced Compression Flanges" (2012). *International Specialty Conference on Cold-Formed Steel Structures. 2.* <https://scholarsmine.mst.edu/isccss/21iccfss/21iccfss-session6/2>

This Article - Conference proceedings is brought to you for free and open access by Scholars' Mine. It has been accepted for inclusion in International Specialty Conference on Cold-Formed Steel Structures by an authorized administrator of Scholars' Mine. This work is protected by U. S. Copyright Law. Unauthorized use including reproduction for redistribution requires the permission of the copyright holder. For more information, please contact scholarsmine@mst.edu.

Direct Strength Design of Metal Building Wall and Roof Systems – Through-Fastened Simple Span Girts and Purlins with Laterally Unbraced Compression Flanges

Tian Gao¹, Christopher D. Moen²

Abstract

A Direct Strength Method (DSM) prediction approach is introduced and validated for metal building wall and roof systems constructed with steel panels through-fastened with screws to girts or purlins. The focus is capacity prediction for simple spans under wind uplift or suction, however the DSM framework is generally formulated to accommodate gravity loads, continuous spans, standing seam roofs, and insulated roof and wall systems in the future. System flexural capacity is calculated with the usual DSM approach – global buckling, local-global buckling interaction, and distortional buckling strengths are determined with a finite strip eigen-buckling analysis including a rotational spring that simulates restraint provided by the through-fastened steel panel. The DSM flexural capacity is then reduced with a code-friendly equation consistent with existing Eurocode provisions to account for the additional stress at the intersection of the web and free flange that occurs as the girt or purlin rotates under a suction (uplift) load. A database of 62 simple span tests was assembled to evaluate strength prediction accuracy of the proposed DSM approach alongside existing Eurocode and American Iron and Steel Institute (AISI) provisions. The proposed DSM approach is confirmed to be viable and accurate for simple spans. Modifications to the Eurocode approach are proposed, and if they are made, the Eurocode is also an accurate and potentially general prediction method. The AISI R-factor prediction method is accurate for C-section simple spans, unconservative for Z-section simple spans, and overall lacks the generality of the DSM and Eurocode.

Introduction

This paper presents a system capacity prediction method for metal building wall and roof systems constructed with cold-formed steel girts or purlins through-fastened to steel panels. For these systems, uplift or suction loading from wind places a girt or purlin's free unbraced flange in compression as shown for C- and

¹ Graduate Research Asst, Virginia Tech, Blacksburg, VA, 24061, USA. (gaot@vt.edu)

² Assistant Professor, Virginia Tech, Blacksburg, VA, 24061, USA. (cmoen@vt.edu)

Z-sections in Figure 1. Member failure initiates at the midspan intersection of the web and free flange from a combination of restrained lateral-torsional buckling deformation and cross-section distortion and rotation caused by strong-axis flexure-induced shear flow (Winter et al. 1949; Zetlin and Winter 1955; Vieira et al. 2010). The cross-section center of twist, treated as the shear center for C- and Z-sections on their own (Seely et al. 1930), changes locations when a girt or purlin is through-fastened to a metal panel (see Figure 1) which has implications for flexural strength prediction that will be discussed herein.

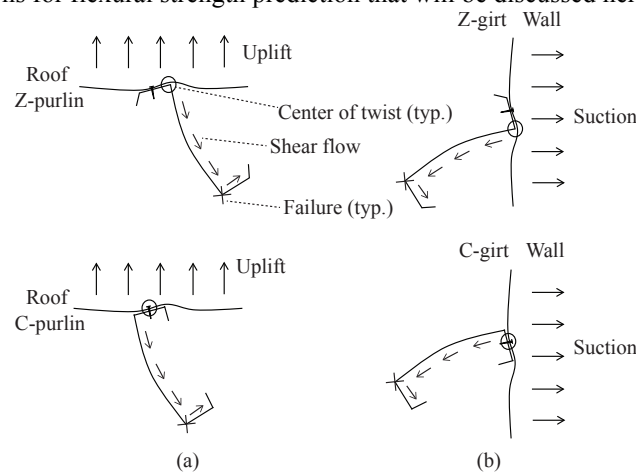


Figure 1. (a) purlin with wind uplift loading; (b) girt with wind suction loading

Through-fastened wall and roof system design approaches are semi-analytical in Europe and experimentally based in North America, Australia, and New Zealand. The European approach (EN-1993 2006) is motivated by a mechanics-based model by Winter and Zetlin (1955) and strength prediction approaches by Douty (1962) and Peköz and Soroushian (1982) which were validated experimentally (e.g., LaBoube 1983) and with computational simulations (e.g., Rousch and Hancock 1997). Widespread use of the Eurocode approach is limited though because of the perceived complexity of the analysis method and because the rotational restraint provided by the metal panel to the cross-section, an important part of a wall or roof system strength prediction procedure, could historically only be quantified by conducting experiments (LaBoube 1986; Rousch and Hancock 1996).

In North America, Australia, and New Zealand (AISI 2007; AS/NZS-4600 2005), wall and roof system wind uplift (suction) capacity prediction is calculated with an experimentally derived knock down factor, i.e., the R-factor, applied to the nominal flexural capacity (Fisher 1996). The R-factor decreases

with increasing cross-section depth and is applicable within prequalified ranges of cross-section dimensions and metal panel thicknesses.

Recent research has demonstrated that the R-factor approach may not be accurate for cases where other limit states govern system strength (Gao and Moen 2012a,), for example, fasteners pulling through the metal panels as the girt or purlin deforms under load. Also, the R-factor approach cannot accommodate other types of wall panel configurations, for example, when rigid board insulation is sandwiched between the wall panel and through-fastened flange.

The goal of this paper is to propose a general system strength approach for metal building wall and roof systems that leverages recent advances in cold-formed steel design through the Direct Strength Method (DSM) (AISI 2007). The work presented here focuses on capacity prediction for wind suction (uplift) and simple span girts and purlins, however the ideas and framework are general and can accommodate other limits states and continuous spans in the future. Accuracy of the three strength prediction approaches – R-factor method (AISI and AS/NZS), Eurocode, and the DSM – is evaluated with a database of 62 tests compiled by the first author. An introduction to the three prediction methods is presented in the next section. Dimension notation used in this paper is provided in Figure 2.

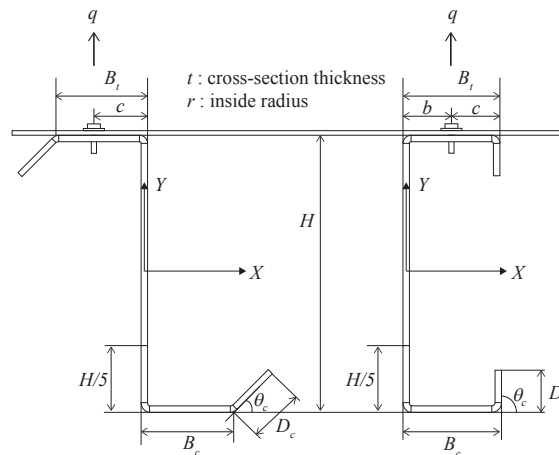


Figure 2. Cross-section dimension notation

R-factor prediction method

Current AISI and AS/NZS prediction methods employ experimentally derived R-factors. In the R-factor method, $M_n = R S_e F_y$, where S_e is the effective section

modulus of the cross-section calculated relative to the extreme compression or tension fiber about the centroidal strong axis, i.e., the X -axis in Figure 2, and F_y is the steel yield stress. The R-factor varies with web depth as shown in Table 1. AS/NZS recommends the use of AISI R-factors for the case when cyclone washers are not used with the fasteners, which is the case assumed in this paper.

Table 1. R-factor (AISI and AS/NZS)

Web depth, mm	Profile	R
$H \leq 165$	C or Z	0.70
$165 < H \leq 216$	C or Z	0.65
$216 < H \leq 292$	Z	0.50
$216 < H \leq 292$	C	0.40

Eurocode prediction method

The Eurocode prediction method (EN-1993 2006) isolates the compressed free girt or purlin flange and a partial web section ($H/5$) from the cross-section (Figure 3a) and treats it as a beam on an elastic foundation (Figure 3b). The lateral force w (force/length) represents the shear flow in the compressed flange from strong axis flexure (see Figure 1) and the foundation spring K (stiffness/length) simulates lateral restraint provided by the web and the through-fastened connection.

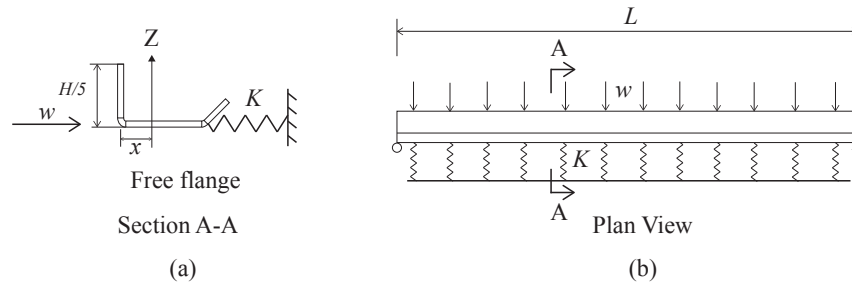


Figure 3. (a) Isolated free flange and partial web; (b) beam on an elastic foundation

Prediction model and interaction equation

The failure stress at the intersection of web and free flange results from a combination of lateral-torsional buckling deformation, i.e., the first term in Eq. (1), and the stress from lateral deformation of the free flange caused by shear flow (σ_f)

$$\frac{1}{\chi_{LT}} \cdot \frac{M_x}{S_e} + \sigma_f \leq F_y \quad (1)$$

where

$$\sigma_f = \frac{M_f}{S_f}. \quad (2)$$

The moment M_x is the required purlin or girt moment capacity and χ_{LT} is the reduction factor for lateral-torsional buckling deformation calculated using European column buckling curve-b. The bending moment in the free flange caused by shear flow is approximated as

$$M_f = k_R \frac{wL^2}{8}. \quad (3)$$

The factor k_R accounts for a moment magnitude reduction in the free flange (Figure 3b) from the distributed spring K

$$k_R = \frac{1-0.0225r}{1+1.013r}, \quad (4)$$

where

$$r = \frac{KL^4}{\pi^4 EI_f} \quad (5)$$

and the flange centroidal strong axis (Z-axis in Figure 3a) moment of inertia is

$$I_f = \left(\frac{Ht^3}{60} + \frac{Htx^2}{5} \right) + \left[\frac{tB_c^3}{12} + B_c t \left(\frac{B_c}{2} - x \right)^2 \right] + \left[\cos^2(\theta_c) \frac{tD_c^2}{12} + D_c t \left(B_c + \frac{\cos(\theta_c)D_c}{2} - x \right)^2 \right]. \quad (6)$$

The origin of Eq. (4) is unknown, however it was established through personal communication (Peköz 2012) that it is an approximation of an exact solution. The authors of this paper confirmed the equation's accuracy with a computer structural analysis parameter study (Gao 2012).

The gross section modulus of the partial web and the free flange, S_f , about the Z-axis in Figure 3a to the compression extreme fiber is

$$S_f = \frac{I_f}{x} \quad (7)$$

where the distance from the centroid to the extreme fiber in compression, x , is

$$x = \frac{B_c^2/2 + B_c D_c + D_c^2 \cos(\theta_c)/2}{H/5 + B_c + D_c}. \quad (8)$$

Equivalent shear flow calculation

The Eurocode calculates the lateral force w for a C-section by assuming the cross-section is a frame with a fixed restraint provided by the panel beyond the fastener as shown in Figure 4a, where the moment reaction $M_r = sH + qb$, and

$s=qB_c t H^2 / (4I_x)$ is the shear flow magnitude in the free flange (Peköz and Soroushian 1982). An equivalent force per length w in the free flange is derived by assuming $M_r = wH$. Solving for w results in

$$w = qk_H, \quad k_H = (B_c t H^2 / 4I_x + b) / H, \quad (9)$$

where q is the uplift (suction) distributed load (force/length) on a purlin or girt, and I_x is the moment of inertia of the cross-section about the X -axis in Figure 2. The out-to-out web depth is H , base metal thickness is t , the free (compressed) flange width is B_c , the flange-stiffener angle is θ_c , and lip stiffener length is D_c as shown in Figure 2.

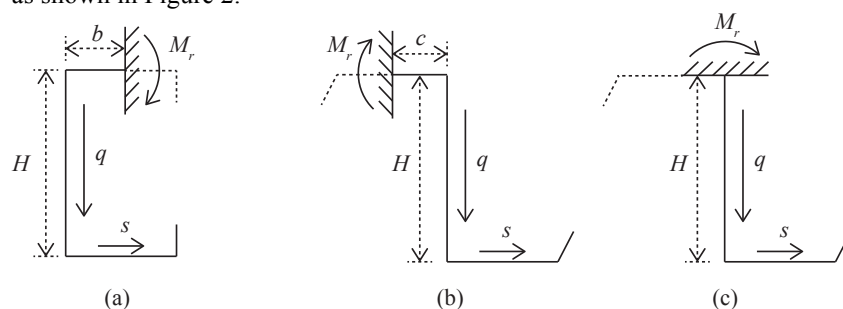


Figure 4. Assumed through-fastened fixity for (a) C-section in Eq. (9); (b) Z-section in Eq. (10); (c) Z-section in Eq. (11)

The Eurocode calculation of the lateral force w for a Z-section in restrained strong axis bending is established with a similar approach to a C-section as shown in Figure 4b. The moment reaction provided by the through-fastened panel is $M_r = sH - qc$ which is assumed equivalent to $M_r = wH$, resulting in

$$w = qk_H, \quad k_H = \frac{Ht(B_c^2 + 2D_c B_c - 2D_c^2 B_c / H)}{4I_x} \frac{c}{H}. \quad (10)$$

A question arises with this derivation though. The fixity location in Figure 4b is not consistent with observed behavior (e.g., Gao and Moen 2012a; Peköz and Soroushian 1982). The cross-section center of rotation is more likely at the web-flange intersection as shown in Figure 4c. For this case, $M_r = sH$ resulting in

$$k_H = \frac{Ht(B_c^2 + 2D_c B_c - 2D_c^2 B_c / H)}{4I_x} \quad (11)$$

This modification to Eq. (10) removes the possibility of negative values for w discussed in the Eurocode. (A negative values can occurs because for some cross-sections the rotation from shear flow in the web dominates over the opposite rotation from shear flow in the flange.) Strength predictions with both approaches, i.e., the use of Eq. (10) vs. Eq. (11), will be compared to test results later in the paper.

Equivalent rotational stiffness calculation

The distributed spring stiffness K has in the past been calculated with empirically derived equations (EN-1993 2006) or obtained from tests (LaBoube 1986; Rousch and Hancock 1996), however for this study K is calculated with recently derived rotational restraint engineering expressions presented in Gao and Moen (2012b).

The stiffness K is obtained by dividing the equivalent shear flow force, w , by the lateral deflection caused by (1) rigid body rotation of the cross-section restrained by the through fastened connection (Δ_1); and (2) cantilever bending of the web about the tension flange-web intersection (Δ_2) as shown in Figure 5.

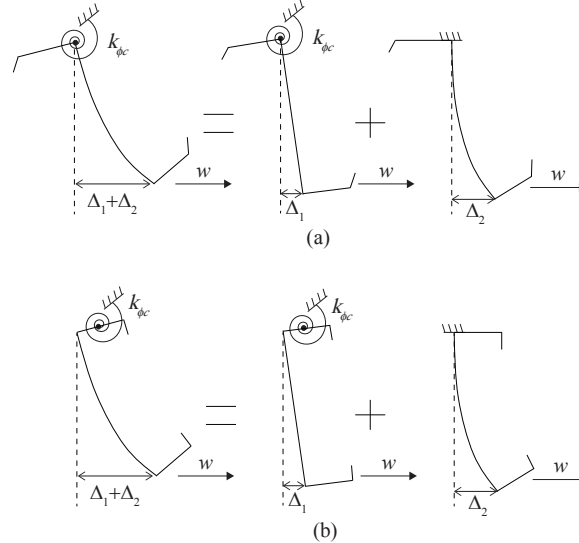


Figure 5. Stiffness K calculation for a (a) Z-section (b) C-section

The equation for K is

$$K = \frac{w}{\Delta_1 + \Delta_2} \quad (12)$$

where

$$\Delta_1 = \frac{wH}{k_{\phi c}} \quad (13)$$

and

$$\Delta_2 = \frac{wH^3}{3EI} \quad (14)$$

The girt or purlin modulus of elasticity is E , $I=t^3/12$ is the unit web bending stiffness treated as a cantilever, and the distributed rotational stiffness $k_{\phi c}$ is calculated as (Gao and Moen 2012b)

$$k_{\phi c} = \left(\frac{S}{c^2 k_p} + \frac{c}{3EI} \right)^{-1}, \quad (15)$$

where S is the fastener spacing and k_p is the panel pull-out stiffness at each fastener calculated with finite element analysis of the panel (Gao 2012). Note that k_p can be tabulated for standard panel cross-sections and fastener locations as discussed in Gao and Moen (2012b). The rotational stiffness in Eq. (15) was originally derived for Z-sections, however it is also used in this paper for C-sections because the flange bending influence, i.e., the second term in Eq. (15), is the same for both Z- and C-sections assuming the C-section through-fastened center of fixity is located as shown in Figure 4a.

The proposed DSM strength prediction approach discussed in the next section merges the Eurocode approach with finite-strip eigenbuckling analysis.

Proposed DSM prediction method

Prediction model and interaction equation

The DSM strength prediction method for through-fastened girts or purlins in uplift or suction employs the interaction equation

$$\frac{M}{S_c} + \sigma_f \leq \frac{M_{ne}}{S_c}, \quad \frac{M}{S_c} + \sigma_f \leq \frac{M_{nt}}{S_c}, \quad (16)$$

where M is the required flexural strength, S_c is the gross strong centroidal axis section modulus for the extreme compression fiber, and σ_f is the flange bending stress due to shear flow calculated with Eq. (2). This approach assumes that girt or purlin failure occurs as lateral-torsional buckling deformation is amplified near peak load by cross-section rotation and distortion from shear flow (Gao and Moen 2012c). The DSM framework is more consistent with physically observed behavior than the Eurocode approach because it addresses local-global buckling interaction of girts or purlins in the calculation of M_{nt} . Also, the global buckling capacity M_{ne} is calculated including the influence of rotational restraint provided by the through-fastened connection (Gao and Moen 2012d).

DSM R-factor derivation for simple span girts and purlins

If M is assumed equal to $R_{DSM}M_{ne}$ for global buckling deformation (or $M=R_{DSM}M_{nt}$ for local-global buckling interaction) where R_{DSM} is a reduction factor that accounts for cross-section deformation from shear flow, then Eqs. (16) can be rewritten as equalities

$$\frac{R_{DSM}M_{ne}}{S_c} = \frac{M_{ne}}{S_c} - \sigma_f, \quad \frac{R_{DSM}M_{nt}}{S_c} = \frac{M_{nt}}{S_c} - \sigma_f. \quad (17)$$

For the specific case considered in this paper – simple span C- and Z-sections, M_f is expanded by substituting $w=qk_H$ into Eq. (3)

$$M_f = k_R k_H \frac{qL^2}{8}. \quad (18)$$

And since $R_{DSM}M_{ne}=qL^2/8$ (or $R_{DSM}M_{nt}=qL^2/8$), then

$$M_f = k_R k_H R_{DSM} M_{ne}, \quad M_f = k_R k_H R_{DSM} M_{nt}. \quad (19)$$

A simple span R_{DSM} factor equation is obtained by substituting Eq. (2) and Eqs. (19) into Eqs. (17), resulting in

$$R_{DSM} = \left(1 + \frac{S_c}{S_f} k_H k_R \right)^{-1}. \quad (20)$$

The flow of a typical DSM calculation is thus preserved in the proposed approach where $M_n = \min(R_{DSM}M_{ne}, R_{DSM}M_{nt}, M_{nd})$. It is assumed that the distortional buckling limit state is not influenced by shear flow and therefore M_{nd} is not multiplied by R_{DSM} . The stress gradient in the compression flange caused by lateral bending from shear flow minimizes the distortional buckling influence.

DSM implementation details – finite strip analysis including rotational restraint

When calculating M_{ne} and M_{nt} from M_{cre} and M_{crl} using finite strip eigen-buckling analysis, the rotational restraint provided by the metal panel to the member's through-fastened flange is simulated by adding a roller and a rotational spring (see Figure 6a) at the cross-section's center of twist (see Figure 1). The rotational spring stiffness is calculated with Eq. (15). The location of the spring in the finite strip analysis should coincide with the cross-section's center of twist when through-fastened to the panel, see Figure 1. The reference stress in the finite strip analysis is calculated assuming restrained bending about the strong centroidal axis as shown in Figure 6b. The critical elastic global buckling moment M_{cre} is multiplied by a moment gradient factor $C_b=1.13$ to account for the parabolic moment diagram in a simple span.

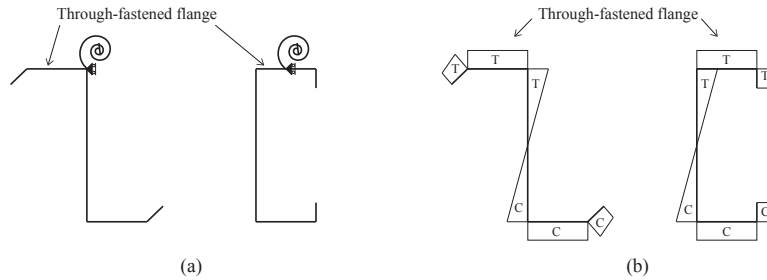


Figure 6. (a) Lateral and rotational restraint; and (b) longitudinal reference stress in a finite strip eigen-buckling analysis

Experimental database

Previous literature was reviewed to collect 62 tested strength data points from 7 simple span pressure box experimental programs as shown in Table 2. All experiments consisted of two parallel C- or Z-section members through-fastened to steel sheeting. The member cross-section dimensions (see Figure 2 for notation), span lengths, steel yield stress, calculated rotational spring stiffness, and tested flexural capacity are summarized in Table A1-A4 in the Appendix of this paper.

Table 2. Experimental program summary

Series	Year	Profile		Panel Thickness (mm)	Panel Rib Depth (mm)	Fastener Location	Imperfection	Boundary Condition
		C	Z					
S1	Peköz and Soroushian (1982)	3	13	0.56	38	Middle	Available	Pin-roller
S2	LaBoube (1983)	4	5	0.46	38	Middle	Available	Bolted
S3	LaBoube (1990)	1	1	0.46	38	Middle	N/A	Bolted
S4	Hancock (1990)	1	1	0.42	29	Crest	N/A	Pin-roller
S5	Rousch and Hancock (1997)	1	1	0.42	29	Crest	N/A	Pin-roller
S6	Fisher (1996)	5	20	0.46	38	Next	N/A	Pin-roller
S7	Gao and Moen (2012a)	2	4	0.46	29	Next	Available	Pin-roller

Fasteners were centered between primary ribs in test series S1 to S3 (Middle), at the primary ribs in S4 and S5 (Crest), and next to the primary ribs in S6 and S7 (Next). The imperfection magnitudes were assumed as zero if not provided. There was no catenary action in test series S1 and S4 to S7 because pin-roller boundary conditions were used. (Pin-roller boundary conditions are consistent with the Eurocode approach and the proposed DSM method). Catenary action was most likely present in test series S2 and S3 because the member tension flange was bolted to both supports.

The fastener location in the flange, i.e., b and c in Figure 2, were measured in test series S7 (and also used when predicting capacity in the following section)

because both rotational restraint (Gao and Moen 2012b) and flexural strength (Gao and Moen 2011) are functions of these dimensions. In test series S1 to S6, it is assumed that the fastener is placed at the center of the flange ($b=c=B_f/2$ in Figure 2). The fastener spacing (S) for all test series was 305mm, and the local panel-fastener stiffness k_p is calculated with second order elastic finite element analysis (see Table A2 in the Appendix).

Test-to-Predicted Comparisons

The average (MEAN), coefficient of variation (COV), and LRFD resistance factor (ϕ) calculated with AISI-S100 Chapter F (AISI 2007) ($\beta=2.5$) are summarized in Table 3 for each of the prediction methods. Elastic buckling and DSM prediction parameters are listed in Table A2 and A3 of the Appendix. The test-to-predicted flexural capacity ratio for each test in the simple span database is provided in the Appendix, Table A4.

Table 3. Test-to-predicted statistics

Prediction Method	M_{test}/M_n								
	C-section (n=17)			Z-section (n=45)			C- and Z-section (n=62)		
	MEAN	COV	ϕ	MEAN	COV	ϕ	MEAN	COV	ϕ
R-factor	1.04	0.15	0.90	0.91	0.18	0.78	0.95	0.18	0.81
Euro Eq. (10)	1.08	0.19	0.91	0.89	0.20	0.75	0.95	0.22	0.79
Euro Eq. (11)	1.08	0.19	0.91	0.96	0.17	0.82	0.99	0.19	0.85
DSM	1.12	0.18	0.95	1.02	0.17	0.88	1.05	0.18	0.90

The R-factor method produces the most accurate strength predictions for C-sections (mean of 1.04 and COV of 0.15), however it is unconservative for Z-sections (mean of 0.91 and COV of 0.18). Considering the complete test database, the R-factor method has an LRFD resistance factor of 0.81 which is lower than $\phi=0.90$ current specified in AISI-S100-07 for flexural members.

The Eurocode approach using Eq. (10) is accurate for C-sections (mean of 1.08 and COV 0.19) but it makes unconservative predictions for Z-sections (mean of 0.89 and COV of 0.20). When using Eq. (11) instead for the Z-section predictions (which removes the web shear flow influence), the test-to-predicted statistics improve both for Z-sections (mean of 0.96 and COV of 0.17) and across the complete database (mean and COV are 0.99 and 0.19). Our findings suggest that the Eurocode prediction accuracy could be improved by replacing Eq. (10) with Eq. (11).

The DSM is also a viable strength prediction approach as demonstrated by the test to predicted mean of 1.05 and a COV of 0.18. The test-to-predicted

statistics result in an LRFD resistance factor of $\phi=0.90$ consistent with the current AISI specification.

Conclusions

A DSM prediction framework is introduced for through-fastened metal building wall and roof systems and validated for the case of simple span C- and Z-section girts and purlins with compression flanges laterally unbraced. The global, local-global, and distortional buckling capacities are determined with a typical DSM calculation using finite strip eigen-buckling analysis. System effects, i.e., girt or purlin interacting with the through-fastened panel, is simulated in a finite strip eigen-buckling analysis with a rotational spring. Then the global buckling and local-global buckling capacities are reduced to account for the longitudinal stresses that occur at the web-free flange intersection as the girt or purlin deforms from shear flow-induced rotation. The rotation occurs about a center of twist defined by the cross-section shape and the type of through-fastened connection.

A newly assembled database of 62 simple span tests was used to evaluate the DSM and compare its accuracy to the existing Eurocode and AISI R-factor methods. The DSM predictions resulted in the highest LRFD resistance factor because of its slightly conservative test-to-predicted mean and the lowest coefficient of variation among the methods evaluated. Modifications are suggested to the existing Eurocode method to improve its prediction accuracy for Z-sections. The existing AISI S100 R-factor prediction approach for simple spans is unconservative for Z-sections, and improvements are needed in AISI-S100-07 Section D6.1 to reach a goal reliability index of 2.5 for through-fastened metal building wall and roof systems.

Girt and purlin design for wind loads has been a broadly studied research area for over 50 years. This is because purlins and girts play a critical role in metal building systems, supporting the exterior building shell and provide out-of-plane bracing to the primary portal frames (Perry et al. 1990). The research presented herein lays the groundwork for a metal building strength prediction framework employing the DSM that can accommodate gravity loads or wind loads, simple spans and continuous spans, standing seam roofs, and insulated roof and wall systems in the future.

Acknowledgements

The authors are grateful to MBMA and AISI for supporting and guiding this work. We offer a special thanks to Dr. Lee Shoemaker and Dr. Teoman Peköz for sharing their valuable historical perspectives on girt and purlin research. This paper was written with support from an MBMA Faculty Fellowship.

References

- AISI. (2007). "AISI S100-07 North American Specification for the Design of Cold-Formed Steel Structural Members." American Iron and Steel Institute, Washington, D.C.
- AS/NZS-4600. (2005). "Australian/New Zealand Standard: Cold-formed Steel Structures."
- Douty, R.T., (1962) "A Design Approach to the Strength of Laterally Unbraced Compression Flanges." Bulletin No. 37, Cornell University Engineering Experiment Station.
- EN-1993-1-3. (2006). "Eurocode 3: Design of Steel Structures. European Committee for Standardization." Brussels, Belgium.
- Fisher, J.M. (1996). "Uplift Capacity of Simple Span Cee and Zee Members with Through-fastened Roof Panels." Final report: MBMA 95-01. Metal Building Manufacturers Association, Cleveland, OH.
- Gao, T. (2012). "Limit State Design of Metal Building Roof and Wall Systems Loaded in Wind Uplift or Suction." Ph.D. Dissertation, Virginia Tech, Blacksburg, VA.
- Gao, T., Moen, C.D. (2011). "Flexural Strength of Exterior Metal Building Wall Assemblies with Rigid Insulation." Virginia Tech Research Report No. CE/VPI-ST-11/01, Blacksburg, VA.
- Gao, T., Moen, C.D. (2012a). "Flexural Strength Experiments on Exterior Metal Building Wall Assemblies with Rigid Insulation." *Journal of Constructional Steel Research* (to appear).
- Gao, T., Moen, C.D. (2012b). "Predicting Rotational Restraint Provided to Wall Girts and Roof Purlins by Through-Fastened Metal Panels." *Thin-Walled Structures* (to appear).
- Gao, T., Moen, C.D. (2012c). "Test Videos-Flexural Strength Experiments on Exterior Metal Building Wall Assemblies with Rigid Insulation." Virginia Tech, Blacksburg, VA. <<http://hdl.handle.net/10919/18714>>.
- Gao, T., Moen, C.D. (2012d). "Flexural Strength of Exterior Metal Building Wall Assemblies with Rigid Insulation." *Proc., Annual Stability Conference Structural Stability Research Council*, Grapevine, TX.
- Hancock, G.J. (1990). "Tests of Purlins with Screw Fastened Sheeting under Wind Uplift." *Proc., 10th International Specialty Conference on Cold-Formed Steel Structures*, Rolla, MO.
- Laboube, R.A. (1983). "Laterally Unsupported Purlins Subjected to Uplift." Report for Metal Building Manufacturers Association, Cleveland, OH.

- LaBoube, R.A. (1986). "Roof Panel to Purlin Connections: Rotational Restraint Factor." *Proc., IABSE Colloquium on Thin-Walled Metal Structures in Buildings*, Stockholm, Sweden.
- LaBoube, R.A., Golovin, M. (1990). "Uplift Behavior of Purlin Systems Having Discrete Braces." *Proc., 10th International Specialty Conference on Cold-Formed Steel Structures*, Rolla, MO.
- Lucas, R.M., Al-Bermani, F.G.A., Kitipornchai S. (1997) "Modelling of Cold-Formed Purlin Sheeting Systems. Part 1: Full model." *Thin-Walled Structures*; 27(3), 223-243.
- Peköz, Teoman, personal communication, June 6, 2012.
- Peköz, T., Soroushian, P. (1982). "Behavior of C- and Z-Purlins under Wind uplift." *Proc., 6th International Specialty Conference on Cold-Formed Steel Structures*, Rolla, MO.
- Perry, D.C., McDonald, J.R., Saffir, H.S. (1990). "Performance of Metal Buildings in High Winds." *Journal of Wind Engineering and Industrial Aerodynamics*; 36(2), 985-999.
- Rousch, C.J., Hancock, G.J. (1996). "Purlin-sheeting Connection Tests." Research report R724, School of Civil and Mining Engineering, The University of Sydney, Australia.
- Rousch, C.J., Hancock, G.J. (1997). "Comparison of Tests of Bridged and Unbridged Purlins with a Non-linear Analysis Model." *Journal of Constructional Steel Research*; 41(2-3), 197-220.
- Schafer, B.W., Adany, S. (2006). "Buckling Analysis of Cold-formed Steel Members Using CUFSM: Conventional and Constrained Finite Strip Methods." *Proc., 18th International Specialty Conference on Cold-Formed Steel Structures*, Orlando, FL.
- Seely, F.B., Putnam, W.J., Schwalbe, W.L. (1930). "The Torsional Effect of Transverse Bending Loads on Channel Beams." *Engineering Experiment Station*; 211, University of Illinois, Urbana.
- Vieira, L.C.M., Malite, M., Schafer, B.W. (2010). "Simplified Models for Cross-section Stress Demands on C-section Purlins in Uplift." *Thin-Walled Structures*; 48(1), 33-41.
- Winter, G., Lansing, W., McCalley, R.B. (1949). "Performance of Laterally Loaded Channel Beams." *Engineering Structures Supplement, Colston Papers*; 2, 179-190.
- Zetlin, L., Winter, G. (1955). "Unsymmetrical Bending of Beams with and without Lateral Bracing." *ASCE Journal of Structural Division*; 81, 774-1.

Appendix Table A1. Specimen cross-section dimensions and yield stress

Test #	Profile	D_z (mm)	B_z (mm)	θ_z (deg.)	H (mm)	D_l (mm)	B_l (mm)	θ_l (deg.)	r (mm)	t (mm)	F_y (MPa)
S1-1	Z	32.0	82.2	36	203.2	32.0	82.2	36	14.7	1.50	455
S1-2	Z	25.4	69.3	40	201.2	25.4	69.3	40	7.6	1.52	424
S1-3	Z	24.0	69.7	50	204.6	24.0	69.7	50	7.1	1.60	393
S1-4	Z	34.6	78.0	40	202.4	34.6	78.0	40	13.4	1.78	446
S1-5	Z	34.5	79.8	41	203.2	34.5	79.8	41	14.0	1.91	446
S1-6	Z	32.4	77.5	41	204.0	32.4	77.5	41	11.7	2.24	440
S1-7	Z	35.2	79.0	43	203.2	35.2	79.0	43	12.6	2.26	442
S1-8	Z	30.4	73.6	48	201.7	30.4	73.6	48	7.8	2.90	387
S1-9	Z	34.8	75.7	36	201.4	34.8	75.7	36	11.3	2.92	455
S1-10	Z	34.0	78.0	46	244.5	34.0	78.0	46	10.2	1.57	396
S1-11	Z	25.1	71.3	42	240.0	25.1	71.3	42	8.3	1.60	395
S1-12	Z	27.3	78.4	41	243.3	27.3	78.4	41	9.3	2.69	365
S1-13	Z	34.3	74.1	40	241.0	34.3	74.1	40	8.6	2.77	397
S1-14	C	21.3	66.5	90	177.8	21.3	66.5	90	10.3	1.91	380
S1-15	C	21.0	63.8	90	228.6	21.0	63.8	90	7.8	1.91	381
S1-16	C	20.7	66.3	90	228.6	20.7	66.3	90	8.1	1.96	381
S2-1	C	19.1	71.4	90	242.8	20.6	71.4	90	8.0	1.80	445
S2-2	C	20.6	71.4	90	241.3	20.6	69.9	90	8.0	1.80	445
S2-3	Z	22.4	69.9	90	241.3	22.4	71.4	90	8.0	1.80	445
S2-4	Z	20.6	69.9	90	241.3	20.6	69.9	90	8.0	1.80	445
S2-5	Z	19.1	71.4	90	244.6	20.6	69.9	90	8.0	1.80	445
S2-6	C	20.6	71.4	90	241.3	20.6	71.4	90	8.0	2.69	445
S2-7	C	20.6	73.2	90	242.8	20.6	71.4	90	8.0	2.69	445
S2-8	Z	20.6	73.2	90	239.8	20.6	71.4	90	8.0	2.69	445
S2-9	Z	22.4	71.4	90	242.8	20.6	73.2	90	8.0	2.69	445
S3-1	Z	26.9	76.2	77	279.4	31.8	74.7	77	6.4	1.91	425
S3-2	C	22.2	88.9	91	292.1	25.4	88.9	91	6.4	2.24	391
S4-1	Z	20.0	74.0	90	205.0	20.0	83.0	90	4.9	2.45	529
S4-2	C	21.3	77.1	90	206.0	21.3	77.1	90	4.9	2.45	518
S5-1	Z	21.5	72.5	90	202.8	21.5	80.7	90	5.0	1.50	527
S5-2	C	20.8	76.7	90	202.0	20.8	76.7	90	5.0	1.50	548
S6-1	Z	22.9	55.9	51	204.5	26.7	57.2	55	5.2	2.60	405
S6-2	Z	20.3	58.4	54	203.2	25.4	57.2	56	5.2	2.60	407
S6-3	Z	21.6	58.4	52	201.9	25.4	54.6	49	5.2	2.61	408
S6-4	Z	21.6	58.4	50	203.2	26.7	54.6	47	5.2	2.61	406
S6-5	Z	17.8	49.5	47	163.8	15.2	48.3	44	3.1	1.54	411
S6-6	Z	16.5	47.0	43	163.8	17.8	50.8	48	3.1	1.55	422
S6-7	Z	24.1	59.7	51	204.5	24.1	50.8	50	3.0	1.52	437
S6-8	Z	22.9	57.2	49	205.7	25.4	52.1	50	3.6	1.79	400
S6-9	Z	26.7	67.3	43	241.3	27.9	67.3	39	3.3	1.67	431
S6-10	Z	25.4	68.6	49	240.0	27.9	68.6	47	3.7	1.87	420
S6-11	Z	22.9	90.2	38	292.1	21.6	91.4	53	4.2	2.10	386
S6-12	C	20.3	62.2	90	163.8	20.3	63.5	90	3.0	1.52	427
S6-13	C	21.6	62.2	88	163.1	21.6	63.5	87	3.0	1.52	428
S6-14	C	17.8	63.5	93	204.5	21.6	62.2	95	3.1	1.53	420
S6-15	C	17.8	63.5	91	203.2	20.3	63.5	90	3.9	1.93	408
S6-16	Z	16.5	48.3	41	163.8	20.3	48.3	43	4.2	2.10	431
S6-17	C	26.7	62.2	87	162.6	24.1	63.5	88	4.2	2.09	421
S6-18	Z	25.4	68.6	52	200.7	27.9	66.0	48	4.1	2.05	428
S6-19	Z	24.1	68.6	50	200.7	26.7	67.3	51	4.1	2.07	391
S6-20	Z	25.4	66.0	45	200.7	26.7	67.3	50	4.2	2.08	400
S6-21	Z	25.4	68.6	48	200.7	25.4	67.3	48	4.2	2.08	335
S6-22	Z	25.4	68.6	51	200.7	26.7	66.0	50	4.1	2.06	405
S6-23	Z	25.4	68.6	51	200.7	25.4	67.3	47	4.2	2.08	411
S6-24	Z	25.4	68.6	53	200.7	25.4	67.3	49	4.1	2.07	404
S6-25	Z	25.4	68.6	46	200.7	25.4	67.3	48	4.1	2.05	419
S7-1	Z	19.8	71.9	55	254.0	20.3	71.9	46	7.1	1.52	404
S7-2	Z	20.8	71.9	55	254.0	21.3	72.6	48	6.4	1.52	401
S7-3	Z	21.1	71.6	55	254.0	22.1	72.9	47	5.8	1.52	402
S7-4	Z	22.4	70.6	54	254.0	20.3	73.2	47	6.1	1.52	399
S7-5	C	20.8	64.5	90	254.0	19.6	65.5	90	5.6	1.52	423
S7-6	C	20.8	64.0	90	254.0	19.3	65.0	90	5.6	1.52	414

Table A2. Span length and finite strip analysis results

Test #	L (mm)	k_p (N/mm)	$k_{\theta c}$ (N-mm/rad/mm)	M_{cr} (kN-mm)	M_{crd} (kN-mm)	M_{ore} (kN-mm)	L_{ore} (mm)
S1-1	6096	257	1061	14332	6684	9050	4064
S1-2	6096	303	972	11468	7358	8239	4064
S1-3	6096	302	1002	12981	9522	8936	4064
S1-4	6096	272	1146	21795	11531	11631	4064
S1-5	6096	266	1199	26989	13457	12900	4064
S1-6	6096	274	1236	39218	18517	15161	4064
S1-7	6096	268	1259	42026	20658	16052	4064
S1-8	6096	288	1232	77922	36979	19104	4064
S1-9	6096	280	1268	31736	N.A.	19343	4064
S1-10	6096	272	1072	12866	11490	10939	4679
S1-11	6096	296	1020	12195	9319	9226	4679
S1-12	6096	271	1295	28932	N.A.	18969	4679
S1-13	6096	286	1235	64890	35355	19886	4679
S1-14	6096	314	1027	24206	17949	10007	3529
S1-15	6096	323	983	20046	20923	9777	4064
S1-16	6096	314	1031	22004	21632	10580	4064
S2-1	6096	214	808	17018	17143	9534	4679
S2-2	6096	219	796	17403	18110	9658	4679
S2-3	6096	214	808	17283	19701	10161	4679
S2-4	6096	219	796	17184	18420	9897	4679
S2-5	6096	219	796	17027	17332	9931	4679
S2-6	6096	214	867	55914	42705	15078	4679
S2-7	6096	214	867	56521	42487	15456	4679
S2-8	6096	214	867	56890	42310	15372	4679
S2-9	6096	208	882	56441	45784	15506	4679
S3-1	9144	202	843	19638	24121	12658	5387
S3-2	9144	152	917	32000	30818	16832	6203
S4-1	7000	322	1653	43751	30921	18011	3529
S4-2	7000	326	1471	45254	31395	17839	4064
S5-1	7000	324	1230	10402	11900	9258	4064
S5-2	7000	327	1166	10651	10896	8683	4679
S6-1	5843	412	1066	47339	30048	12262	3529
S6-2	5843	412	1066	28610	N.A.	12276	3529
S6-3	5843	417	991	29069	N.A.	12098	3529
S6-4	5843	417	990	28430	N.A.	12077	3529
S6-5	5843	431	743	10877	7149	5404	3065
S6-6	5843	425	803	10300	6725	5212	2662
S6-7	5843	425	799	10946	9658	7336	4064
S6-8	5843	423	867	16710	13019	8458	3529
S6-9	5843	391	1203	13549	11644	10680	4679
S6-10	5843	388	1299	19120	15846	12612	4679
S6-11	5843	341	1904	25867	15464	19787	5387
S6-12	5843	399	1068	11037	10973	7158	3529
S6-13	5843	399	1069	11160	11348	7290	3529
S6-14	5715	402	1047	10511	11403	7238	4064
S6-15	5715	399	1184	21005	18349	10165	3529
S6-16	7367	431	789	12625	N.A.	6832	2662
S6-17	7367	399	1210	28954	25349	12067	3529
S6-18	7367	394	1273	27032	17846	13299	4064
S6-19	7367	391	1311	27358	16956	13357	3529
S6-20	7367	391	1313	27656	16713	13177	3529
S6-21	7367	391	1313	28395	17246	13624	4064
S6-22	7367	394	1275	27602	17780	13370	4064
S6-23	7367	391	1313	28236	18052	13619	4064
S6-24	7367	391	1311	27838	18429	13564	4064
S6-25	7367	391	1307	27067	16125	13364	4064
S7-1	7468	300	958	9937	8810	8320	4679
S7-2	7468	315	826	9963	9303	8273	4679
S7-3	7468	342	634	9936	9499	7850	4679
S7-4	7468	277	1171	10017	9896	8983	4679
S7-5	7468	372	466	9749	13635	6321	5387
S7-6	7468	326	740	9727	13646	6986	4679

Table A3. Test to predicted comparison - DSM

Test #	S_c (mm ²)	S_f (mm ³)	k_R	k_H	R_{DSM}	M_{ne} (kN-mm)	M_{nc} (kN-mm)	M_{nd} (kN-mm)	M_y (kN-mm)	M_n (kN-mm)	M_{test} (kN-mm)	M_{test}/M_n
S1-1	40129	7595	0.27	0.21	0.77	9050	8916	9580	18268	6890	6200	0.90
S1-2	35902	5898	0.17	0.17	0.85	8239	7794	8967	15230	6618	5600	0.85
S1-3	38034	6058	0.17	0.16	0.85	8890	8538	9826	14925	7284	6500	0.89
S1-4	46192	8659	0.23	0.20	0.80	11627	11627	12869	20582	9329	8000	0.86
S1-5	50128	9498	0.23	0.21	0.80	12882	12882	14390	22371	10298	9400	0.91
S1-6	57632	10604	0.21	0.20	0.82	15085	15085	17597	25361	12339	11200	0.91
S1-7	59026	11163	0.22	0.21	0.81	15897	15897	18656	26057	12827	11000	0.86
S1-8	70138	12412	0.19	0.19	0.83	18256	18256	23544	27140	15218	14500	0.95
S1-9	73529	13949	0.22	0.20	0.81	19312	19247	N.A.	33422	15672	12500	0.80
S1-10	52950	8443	0.36	0.16	0.74	10939	9804	12998	20978	7244	8100	1.12
S1-11	48189	7109	0.27	0.14	0.80	9226	8585	11272	19046	6877	7700	1.12
S1-12	86271	13683	0.28	0.16	0.79	18854	18393	N.A.	31478	14446	18100	1.25
S1-13	88172	14239	0.29	0.15	0.78	19877	19877	27414	35031	15520	14800	0.95
S1-14	33107	5542	0.08	0.31	0.87	9090	9090	11066	12559	7931	8600	1.08
S1-15	46557	6245	0.15	0.22	0.80	9777	9777	14664	17742	7844	7900	1.01
S1-16	48622	6696	0.16	0.23	0.79	10572	10572	15262	18529	8368	7000	0.84
S2-1	50938	6958	0.24	0.24	0.71	9534	9534	15934	22651	6769	7100	1.05
S2-2	50400	6991	0.24	0.24	0.71	9658	9658	16162	22412	6870	6800	0.99
S2-3	50921	6883	0.23	0.14	0.81	10161	10161	16787	22644	8226	8400	1.02
S2-4	50072	6815	0.23	0.14	0.81	9897	9897	16200	22266	8062	9200	1.14
S2-5	51121	6994	0.24	0.13	0.81	9931	9931	16037	22733	8034	8200	1.02
S2-6	74063	10439	0.24	0.24	0.71	15078	15078	28108	32934	10685	13400	1.25
S2-7	75281	10793	0.26	0.24	0.70	15456	15456	28366	33476	10792	14300	1.33
S2-8	73971	10699	0.25	0.15	0.80	15372	15372	27998	32894	12259	15900	1.30
S2-9	75675	10589	0.25	0.14	0.80	15506	15506	29179	33652	12398	16500	1.33
S3-1	72526	9447	0.10	0.13	0.92	12658	12391	21957	30815	11352	17700	1.56
S3-2	94906	12936	0.13	0.24	0.81	16832	16832	27041	37116	13663	19500	1.43
S4-1	58775	8847	0.06	0.17	0.94	17980	17980	24198	31081	16900	20100	1.19
S4-2	58798	9405	0.07	0.31	0.88	17791	17791	24010	30446	15568	22200	1.43
S5-1	36356	5291	0.08	0.17	0.92	9258	8175	12479	19153	7497	11300	1.51
S5-2	35919	5632	0.09	0.31	0.85	8683	7888	12245	19677	6666	10400	1.56
S6-1	54226	7674	0.12	0.13	0.90	12262	12262	19074	21955	11071	12500	1.13
S6-2	53659	7700	0.12	0.13	0.90	12274	12274	N.A.	21837	11060	12200	1.10
S6-3	53015	7863	0.13	0.14	0.89	12098	12098	N.A.	21612	10797	11800	1.09
S6-4	53951	7917	0.13	0.14	0.89	12077	12077	N.A.	21881	10762	10400	0.97
S6-5	21485	3238	0.05	0.14	0.96	5358	5358	6374	8833	5129	5300	1.03
S6-6	21765	3053	0.04	0.13	0.97	5209	5209	6375	9173	5045	4900	0.97
S6-7	32443	4892	0.17	0.14	0.86	7336	7094	9581	14187	6130	6100	1.00
S6-8	37905	5455	0.14	0.13	0.89	8458	8458	11187	15164	7508	7800	1.04
S6-9	50510	7112	0.27	0.13	0.81	10680	9809	13362	21775	7904	8300	1.05
S6-10	56157	7903	0.24	0.13	0.82	12612	12257	15847	23589	10022	11200	1.12
S6-11	93333	13388	0.44	0.13	0.71	19787	18348	20188	35986	13028	12800	0.98
S6-12	24502	3841	0.06	0.31	0.89	6905	6823	8300	10461	6072	5600	0.92
S6-13	24615	3885	0.06	0.32	0.89	7008	6916	8442	10543	6141	5900	0.96
S6-14	32974	4495	0.14	0.24	0.80	7238	6939	10059	13851	5577	5600	1.00
S6-15	40784	5670	0.12	0.25	0.83	10083	10083	13444	16653	8345	9900	1.19
S6-16	29077	4270	0.00	0.14	1.00	6832	6832	N.A.	12515	6807	7500	1.10
S6-17	33384	5488	0.01	0.32	0.98	10561	10561	13293	14046	10330	10600	1.03
S6-18	47406	7617	0.05	0.17	0.95	12993	12993	15110	20306	12291	10500	0.85
S6-19	46916	7613	0.05	0.17	0.95	12608	12608	13908	18349	11966	10100	0.84
S6-20	47750	7553	0.05	0.16	0.95	12678	12678	14191	19103	12076	11200	0.93
S6-21	48140	7815	0.05	0.17	0.95	12018	12018	12871	16104	11381	9900	0.87
S6-22	47498	7684	0.05	0.17	0.95	12830	12830	14580	19231	12137	10500	0.87
S6-23	47988	7740	0.05	0.17	0.95	13100	13100	14900	19727	12409	9600	0.77
S6-24	47680	7664	0.05	0.17	0.95	12962	12962	14791	19272	12280	9900	0.81
S6-25	47447	7727	0.06	0.17	0.95	12959	12959	14350	19865	12265	9900	0.81
S7-1	48309	6540	0.14	0.12	0.89	8320	7494	11165	19490	6647	7100	1.07
S7-2	48873	6611	0.15	0.12	0.88	8273	7471	11450	19582	6556	7000	1.07
S7-3	49135	6602	0.17	0.12	0.86	7850	7204	11600	19728	6224	6800	1.09
S7-4	48876	6601	0.13	0.12	0.89	8983	7913	11719	19513	7063	7300	1.03
S7-5	44609	5455	0.15	0.25	0.77	6321	6176	13037	18861	4745	5200	1.10
S7-6	44379	5406	0.11	0.22	0.83	6986	6609	12837	18385	5509	5200	0.94

$$M_n = \min(R_{DSM} M_{ne}, R_{DSM} M_{nc}, M_{nd})$$

Table A4. Test-to-predicted comparison – all methods

Test #	R-factor	M_{test}/M_n		
		Euro Eq. (10)	Euro Eq. (11)	DSM
S1-1	0.64	0.59	0.69	0.90
S1-2	0.70	0.70	0.76	0.85
S1-3	0.77	0.79	0.86	0.89
S1-4	0.69	0.64	0.73	0.86
S1-5	0.73	0.67	0.77	0.91
S1-6	0.76	0.70	0.79	0.91
S1-7	0.70	0.64	0.73	0.86
S1-8	0.82	0.78	0.89	0.95
S1-9	0.58	0.53	0.61	0.80
S1-10	0.96	0.76	0.90	1.12
S1-11	1.00	0.85	0.94	1.12
S1-12	1.19	0.92	1.07	1.25
S1-13	0.85	0.66	0.77	0.95
S1-14	1.12	1.25	1.25	1.08
S1-15	1.18	1.00	1.00	1.01
S1-16	1.01	0.84	0.84	0.84
S2-1	0.95	0.86	0.86	1.05
S2-2	0.89	0.81	0.81	0.99
S2-3	0.87	0.82	0.90	1.02
S2-4	0.98	0.92	1.01	1.14
S2-5	0.87	0.82	0.89	1.02
S2-6	1.06	0.99	0.99	1.25
S2-7	1.12	1.05	1.05	1.33
S2-8	1.02	0.93	1.05	1.30
S2-9	1.02	0.95	1.06	1.33
S3-1	1.36	1.45	1.50	1.56
S3-2	1.26	1.42	1.42	1.43
S4-1	1.22	1.22	1.25	1.19
S4-2	1.37	1.48	1.48	1.43
S5-1	1.29	1.39	1.43	1.51
S5-2	1.18	1.35	1.35	1.56
S6-1	0.89	0.98	1.03	1.13
S6-2	0.86	0.94	1.00	1.10
S6-3	0.84	0.92	0.98	1.09
S6-4	0.74	0.80	0.86	0.97
S6-5	0.97	1.13	1.16	1.03
S6-6	0.89	1.05	1.06	0.97
S6-7	0.75	0.84	0.90	1.00
S6-8	0.85	0.94	1.00	1.04
S6-9	0.98	0.82	0.91	1.05
S6-10	1.12	0.92	1.01	1.12
S6-11	0.97	0.79	0.90	0.98
S6-12	0.88	1.02	1.02	0.92
S6-13	0.90	1.04	1.04	0.96
S6-14	0.78	0.99	0.99	1.00
S6-15	1.05	1.27	1.27	1.19
S6-16	0.90	1.12	1.12	1.10
S6-17	1.09	1.18	1.18	1.03
S6-18	0.90	0.90	0.93	0.85
S6-19	0.95	0.95	0.98	0.84
S6-20	1.01	1.02	1.04	0.93
S6-21	0.98	0.98	1.01	0.87
S6-22	0.94	0.94	0.98	0.87
S6-23	0.84	0.84	0.87	0.77
S6-24	0.88	0.88	0.91	0.81
S6-25	0.87	0.87	0.90	0.81
S7-1	1.01	0.98	1.02	1.07
S7-2	0.96	0.94	0.99	1.07
S7-3	0.93	0.96	1.00	1.09
S7-4	0.99	0.95	0.98	1.03
S7-5	0.89	0.95	0.95	1.10
S7-6	0.91	0.88	0.88	0.94